

Viability of light-Higgs strongly-coupled scenarios

Juan José Sanz-Cillero^{*†}

Departamento de Física Teórica and Instituto de Física Teórica, IFT-UAM/CSIC, Universidad Autónoma de Madrid, Cantoblanco, E-28049 Madrid, Spain
E-mail: juanj.sanz@uam.es

Antonio Pich

Departament de Física Teòrica, IFIC, Universitat de València – CSIC
Apt. Correus 22085, E-46071 València, Spain
E-mail: pich@ific.uv.es

Ignasi Rosell

Departamento de Ciencias Físicas, Matemáticas y de la Computación, ESET, Universidad CEU Cardenal Herrera, E-46115 Alfara del Patriarca, València, Spain
E-mail: rosell@uch.ceu.es

Contrary to what is sometimes stated, the current electroweak precision data easily allow for massive composite resonance states at the natural EW scale, *i.e.*, well over the TeV. The oblique parameters S and T are analyzed by means of an effective Lagrangian that implements the $SU(2)_L \otimes SU(2)_R \rightarrow SU(2)_{L+R}$ pattern of electroweak symmetry breaking. They are computed at the one-loop level and incorporating the newly discovered Higgs-like boson and possible spin-1 composite resonances. Imposing a proper ultraviolet behaviour is crucial and allows us to determine S and T at next-to-leading order in terms of a few resonance parameters. Electroweak precision data force the vector and axial-vector states to have masses above the TeV scale and suggest that the W^+W^- and ZZ couplings to the Higgs-like scalar should be close to the Standard Model value. Our findings are generic: they only rely on symmetry principles and soft requirements on the short-distance properties of the underlying strongly-coupled theory, which are widely satisfied in more specific scenarios.

The European Physical Society Conference on High Energy Physics -EPS-HEP2013
18-24 July 2013
Stockholm, Sweden

^{*}Speaker.

[†]Work supported in part by the Spanish Government and ERDF funds from the European Commission [FPA2010-17747, FPA2011-23778, AIC-D-2011-0818, SEV-2012-0249, CSD2007-00042], the Generalitat Valenciana [PrometeoII/2013/007] and the Comunidad de Madrid [HEPHACOS S2009/ESP-1473].

1. Introduction

In this talk we present the first combined analysis of the oblique parameters S and T [1, 2], including the newly discovered Higgs-like boson and possible spin-1 composite resonances at the one-loop level [3, 4]. We consider a general Lagrangian implementing the $SU(2)_L \otimes SU(2)_R \rightarrow SU(2)_{L+R}$ pattern of electroweak symmetry breaking (EWSB), with a non-linear realization of the corresponding Goldstone bosons [5]. We consider strongly-coupled models where the gauge symmetry is dynamically broken by means of some non-perturbative interaction. Usually, theories of this kind do not contain a fundamental Higgs, bringing instead composite states of different types, in a similar way as it happens in Quantum Chromodynamics. In the past, electroweak (EW) chiral effective Lagrangians [5] were used for the study of the oblique parameters [6]. In the recent years, several works have incorporated vector and axial-vector resonances and performed one-loop computations of S and T within a similar $SU(2)_L \otimes SU(2)_R/SU(2)_{L+R}$ effective framework [7, 8]. However, they contained unphysical dependences on the ultraviolet (UV) cut-off, manifesting the need for local contributions to account for a proper UV completion. Our calculation avoids this problem through the implementation of short-distance conditions on the relevant Green functions, in order to satisfy the assumed UV behaviour of the strongly-coupled theory. As shown in Refs. [9, 10], the dispersive approach we adopt avoids all technicalities associated with the renormalization procedure, allowing for a much more transparent understanding of the underlying physics.

2. Electroweak effective theory

Let us consider a low-energy effective theory containing the Standard Model (SM) gauge bosons coupled to the EW Goldstones, one scalar state S_1 with mass $m_{S_1} = 126$ GeV and the lightest vector and axial-vector resonance multiplets V and A , which are expected to be the most relevant ones at low energies. We assume the SM pattern of EWSB and the scalar field S_1 is taken to be a singlet, whereas V and A are introduced as triplets.

The relevant one-loop absorptive diagrams we will compute require interaction vertices with at most three legs. In addition, since we just consider contributions from the lightest channels, $\phi\phi$ (two Goldstones) and $S_1\phi$ for the S -parameter, and ϕB and $S_1 B$ for T , we will just need the Lagrangian operators [3, 4]

$$\begin{aligned} \mathcal{L} = & \left(1 + \frac{2\kappa_W}{v} S_1\right) \frac{v^2}{4} \langle u_\mu u^\mu \rangle + \frac{F_V}{2\sqrt{2}} \langle V_{\mu\nu} f_+^{\mu\nu} \rangle + \frac{iG_V}{2\sqrt{2}} \langle V_{\mu\nu} [u^\mu, u^\nu] \rangle \\ & + \frac{F_A}{2\sqrt{2}} \langle A_{\mu\nu} f_-^{\mu\nu} \rangle + \sqrt{2} \lambda_1^{SA} \partial_\mu S_1 \langle A^{\mu\nu} u_\nu \rangle, \end{aligned} \quad (2.1)$$

with $u_\mu = -\vec{\sigma} \partial_\mu \vec{\phi}/v + \dots$ and the other chiral tensors are defined in [4, 11]. In addition, we will have the Yang-Mills and gauge-fixing terms, with the computation performed in the Landau gauge. The term proportional to κ_W in Eq. (2.1) contains the coupling of the scalar S_1 resonance to two gauge bosons. For $\kappa_W = 1$ one recovers the $S_1 \rightarrow \phi\phi$ vertex of the SM. The computation is performed in the Landau gauge.

3. Oblique parameters

The S -parameter measures the difference between the off-diagonal $W^3 B$ correlator and its SM value, while T parametrizes the breaking of custodial symmetry [1]:

$$S = \frac{16\pi}{g^2} (e_3 - e_3^{\text{SM}}), \quad T = \frac{4\pi}{g^2 \sin^2 \theta_W} (e_1 - e_1^{\text{SM}}), \quad (3.1)$$

with

$$e_3 = \frac{g}{g'} \tilde{\Pi}_{30}(0), \quad e_1 = \frac{1}{M_W^2} (\Pi_{33}(0) - \Pi_{WW}(0)). \quad (3.2)$$

The tree-level Goldstone contribution in e_3 has been removed from $\Pi_{30}(q^2)$ in the form $\Pi_{30}(q^2) = q^2 \tilde{\Pi}_{30}(q^2) + g^2 \tan \theta_W v^2/4$. For the computation of these oblique parameters we have made use of the dispersive representations [1, 3, 4]

$$S = \frac{16\pi}{g^2 \tan \theta_W} \int_0^\infty \frac{dt}{t} [\rho_S(t) - \rho_S(t)^{\text{SM}}], \quad (3.3)$$

$$T = \frac{4\pi}{g'^2 \cos^2 \theta_W} \int_0^\infty \frac{dt}{t^2} [\rho_T(t) - \rho_T(t)^{\text{SM}}], \quad (3.4)$$

with the one-loop spectral functions (we will remain at lowest order in g and g')

$$\rho_S(t) = \frac{1}{\pi} \text{Im} \tilde{\Pi}_{30}(t), \quad \rho_T(t) = \frac{1}{\pi} \text{Im} [\Sigma(t)^{(0)} - \Sigma(t)^{(+)}]. \quad (3.5)$$

The first dispersion relation (3.3) was worked out by Peskin and Takeuchi [1] and its convergence requires a vanishing spectral function at short distances. Since $\rho_S(t)^{\text{SM}}$ vanishes at high energies, the spectral function $\rho_S(t)$ of the theory we want to analyze must also go to zero for $s \rightarrow \infty$. This removes from the picture any undesired UV cut-off and S depends only on the physical scales of the problem. For the computation of T , we employ the Ward-Takahashi identity [12] which relates the Π_{33} and Π_{WW} polarizations with the EW Goldstone self-energies $\Sigma^{(0)}$ and $\Sigma^{(+)}$, respectively. In the Landau gauge one finds the next-to-leading order (NLO) relation $e_1 = \Sigma'(0)^{(0)} - \Sigma'(0)^{(\pm)}$, with $\Sigma'(t) \equiv \frac{d}{dt} \Sigma(t)$ [3, 4]. We have computed the one-loop contributions to the Goldstone self-energies from the lightest two-particle absorptive cuts: ϕB and $S_1 B$. Our analysis [3, 4] shows that, once proper short-distance conditions have been imposed on the form-factors that determine $\rho_S(t)$, the spectral function $\rho_T(t)$ also vanishes at high momentum and one is allowed to recover T by means of the UV-converging dispersion relation (3.4). Nonetheless, we want to stress that this property, hinted previously by Ref. [8], has only been explicitly checked for the leading channels, ϕB and $S_1 B$, contributing to T . The $1/t$ and $1/t^2$ weights in Eqs. (3.3) and (3.4), respectively, enhance the contribution from the lightest thresholds and suppress channels with heavy states [10]. Thus, in this talk we focus our attention on the lightest one and two-particle cuts: $\phi, V, A, \phi\phi$ and $S_1\phi$ for the S -parameter; ϕB and $S_1 B$ for T . Since the leading-order (LO) determination of S already implies that the vector and axial-vector masses must be above the TeV scale, two-particle cuts with V and A resonances are very suppressed. Their effect was estimated in Ref. [11] and found to be small.

4. Short-distance constraints: Weinberg sum-rules

Since we are assuming that weak isospin and parity are good symmetries of the strong dynamics, the correlator $\Pi_{30}(s)$ can be written in terms of the vector ($R+L$) and axial-vector ($R-L$)

two-point functions as [1]

$$\Pi_{30}(s) = \frac{g^2 \tan \theta_W}{4} s [\Pi_{VV}(s) - \Pi_{AA}(s)]. \quad (4.1)$$

In asymptotically-free gauge theories the difference $\Pi_{VV}(s) - \Pi_{AA}(s)$ vanishes at $s \rightarrow \infty$ as $1/s^3$ [13]. This implies two super-convergent sum rules, known as the 1st and 2nd Weinberg sum-rules (WSRs) [14]. At LO (tree-level), the 1st and 2nd WSRs imply, respectively, [1, 14]

$$F_V^2 - F_A^2 = v^2, \quad F_V^2 M_V^2 - F_A^2 M_A^2 = 0, \quad (4.2)$$

where the 1st (2nd) WSR stems from requiring $\Pi_{VV}(s) - \Pi_{AA}(s)$ to vanish faster than $1/s$ ($1/s^2$) at short distances. If both WSRs are valid, one has $M_V < M_A$ and the vector and axial-vector couplings $F_{V,A}$ can be determined at LO in terms of the resonance masses [1, 3, 4, 15]. On the other hand, if only the 1st WSR is assumed then the vector is no longer forced to be lighter than the axial-vector [16, 17]; all one can say is that $F_V^2 > F_A^2$. It is likely that the 1st WSR is also true in gauge theories with non-trivial UV fixed points [8]. However, the 2nd WSR cannot be used in Conformal Technicolour models [8] and its validity is questionable in most Walking Technicolour scenarios [16].

The $\phi\phi$ and $S_1\phi$ contributions to the spectral function $\rho_S(t)$ are given by

$$\rho_S(s)|_{\phi\phi} = \theta(s) \frac{g^2 \tan \theta_W}{192\pi^2} |\mathcal{F}_{\phi\phi}^v(s)|^2, \quad (4.3)$$

$$\rho_S(s)|_{S_1\phi} = -\theta(s - m_{S_1}^2) \frac{g^2 \tan \theta_W}{192\pi^2} |\mathcal{F}_{S_1\phi}^a(s)|^2 \left(1 - \frac{m_{S_1}^2}{s}\right)^3, \quad (4.4)$$

with the $\phi\phi$ and $S_1\phi$ form-factors, respectively, provided at LO by [3, 4, 10]

$$\mathcal{F}_{\phi\phi}^v(s) = 1 + \sigma_V \frac{s}{M_V^2 - s}, \quad \mathcal{F}_{S_1\phi}^a(s) = \kappa_W \left(1 + \sigma_A \frac{s}{M_A^2 - s}\right), \quad (4.5)$$

with $\sigma_V \equiv F_V G_V / v^2$ and $\sigma_A \equiv F_A \lambda_1^{\text{SA}} / (\kappa_W v)$. We will demand these form factors to fall as $\mathcal{O}(1/s)$, *i.e.*, $\sigma_V = \sigma_A = 1$ [3, 4]. When computing the T parameter at NLO we found that the ϕB and $S_1 B$ channels in the $\rho_T(t)$ spectral function were fully determined by the form-factors $\mathcal{F}_{\phi\phi}^v$ and $\mathcal{F}_{S_1\phi}^a$, respectively [4]. This relation between the $\phi\phi$ vector form-factor and the T -parameter was also previously hinted in Ref. [8]. Thus, in addition to making $\Pi_{30}(t)$ and $\rho_S(t)$ well-behaved at short distances, these conditions alone lead to a good high-energy behaviour for the $\rho_T(t)$ spectral function [3, 4].

5. Theoretical predictions at LO and NLO

At leading order, the tree-level Goldstone self-energies are identically zero and one has $T_{\text{LO}} = 0$. On the other hand, for the S -parameter one obtains [1, 3, 4, 11]

$$S_{\text{LO}} = \frac{4\pi v^2}{M_V^2} \left(1 + \frac{M_V^2}{M_A^2}\right) \quad (\text{Two WSRs}), \quad (5.1)$$

$$S_{\text{LO}} > \frac{4\pi v^2}{M_V^2} \quad (\text{Only the 1st WSRs; } M_V < M_A), \quad (5.2)$$

with the last inequality flipping sign (becoming an identity) in the inverted-mass scenario $M_V > M_A$ [16, 17] (degenerate-mass scenario $M_V = M_A$). Eq. (5.1) assumes the validity of the two WSRs, while only the 1st WSR is taken into account in Eq. (5.2), but assuming $M_V < M_A$. In both cases, the resonance masses need to be heavy enough to comply with the stringent experimental limits on S [2], implying $M_V > 1.5$ TeV (2.3 TeV) at the 3σ (1σ) level.

At NLO, the requirement that $\text{Im}\tilde{\Pi}_{30}(s)$ vanishes at short distances allows us to reconstruct the full correlator $\Pi_{30}(s)$ through a one subtracted dispersion relation [3, 4, 10, 11]:

$$\Pi_{30}(s)|_{\text{NLO}} = \frac{g^2 \tan \theta_W}{4} s \left(\frac{v^2}{s} + \frac{F_V^{r2}}{M_V^{r2} - s} - \frac{F_A^{r2}}{M_A^{r2} - s} + \bar{\Pi}(s) \right), \quad (5.3)$$

with the renormalized F_R^r and M_R^r and the finite one-loop contribution $\bar{\Pi}(s)$, fully determined by $\text{Im}\tilde{\Pi}_{30}(s)$ (see App. A of Ref. [11]). By imposing the WSRs at NLO, one obtains NLO conditions on the high-energy expansion of $\Pi_{30}(s)|_{\text{NLO}}$ in powers of $1/s$. Its real and imaginary parts allow us to constrain the renormalized resonance couplings $F_{V,A}^{r2}$ and produces the condition $\kappa_W = M_V^2/M_A^2$ (in the case with two WSRs), respectively. Thus, for the NLO S -parameter one finds [3, 4]

$$S = 4\pi v^2 \left(\frac{1}{M_V^2} + \frac{1}{M_A^2} \right) + \frac{1}{12\pi} \left[\log \frac{M_V^2}{m_H^2} - \frac{11}{6} + \frac{M_V^2}{M_A^2} \log \frac{M_A^2}{M_V^2} - \frac{M_V^4}{M_A^4} \left(\log \frac{M_A^2}{m_{S_1}^2} - \frac{11}{6} \right) \right] \quad (\text{Two WSRs}), \quad (5.4)$$

$$S > \frac{4\pi v^2}{M_V^2} + \frac{1}{12\pi} \left[\left(\ln \frac{M_V^2}{m_H^2} - \frac{11}{6} \right) - \kappa_W^2 \left(\log \frac{M_A^2}{m_{S_1}^2} - \frac{17}{6} + \frac{M_A^2}{M_V^2} \right) \right] \quad (\text{Only the 1st WSR; } M_V < M_A), \quad (5.5)$$

where m_H sets the reference Higgs mass in the definition of the oblique parameters. We have used the renormalized masses in the NLO expressions and the superscript r is dropped from now on. As in the LO case, in the case $M_V > M_A$ [16, 17] ($M_A = M_V$), the inequality (5.5) flips direction (becomes an identity).

As we saw in the previous section, one also has $\rho_T(t) \xrightarrow{t \rightarrow \infty} 0$ for the ϕB and $S_1 B$ channels once the $\rho_S(t)$ spectral function constraints $\sigma_V = \sigma_A = 1$ are imposed and the form-factors vanish at high energies. The T dispersion relation (3.4) becomes then UV convergent and yields [3, 4]

$$T = \frac{3}{16\pi \cos^2 \theta_W} \left[1 + \log \frac{m_H^2}{M_V^2} - \kappa_W^2 \left(1 + \log \frac{m_{S_1}^2}{M_A^2} \right) \right]. \quad (5.6)$$

Terms of $\mathcal{O}(m_{S_1}^2/M_A^2)$ have been neglected in Eqs. (5.4)–(5.6). After imposing the high-energy constraints, the S and T determinations can be written in terms of two (three) parameters, *e.g.*, M_V and κ_W (M_V , M_A and κ_W), in the case with two WSRs (with only the 1st WSR).

6. Phenomenology

1) Case with two WSRs: In the more restrictive scenario, we find at 68% (95%) CL (Fig. 1):

$$0.97 \text{ (0.94)} < \kappa_W < 1, \quad M_A > M_V > 5 \text{ (4) TeV}. \quad (6.1)$$

As $\kappa_W = M_V^2/M_A^2$ due to the 2nd WSR at NLO, the vector and axial-vector turn out to be quite degenerate.

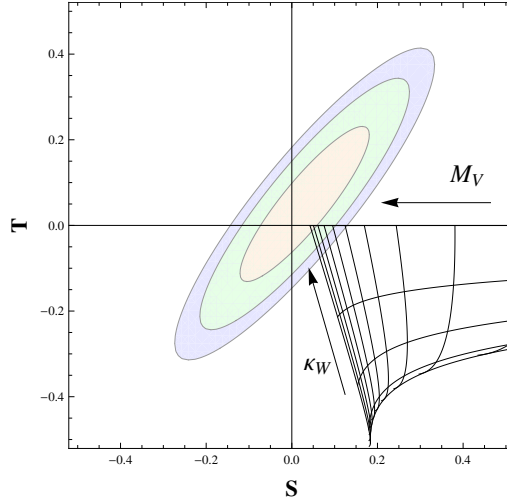


Figure 1: NLO determinations of S and T , imposing the two WSRs. The grid lines correspond to M_V values from 1.5 to 6.0 TeV, at intervals of 0.5 TeV, and $\kappa_W = 0, 0.25, 0.50, 0.75, 1$. The arrows indicate the directions of growing M_V and κ_W . The ellipses give the experimentally allowed regions at 68% (orange), 95% (green) and 99% (blue) CL [2].

2) Case with only the 1st WSR: The previous stringent bounds get softened when only the 1st WSR is required to be valid. On general grounds, one would expect this scenario to satisfy the mass hierarchy $M_V < M_A$. Assuming a moderate splitting $0.5 < M_V/M_A < 1$, we obtain (68% CL)

$$0.84 < \kappa_W < 1.3, \quad M_V > 1.5 \text{ TeV}. \quad (6.2)$$

Slightly larger departures from the SM can be achieved by considering a larger mass splitting.

When the resonance masses become degenerate, the allowed range for the scalar coupling shrinks to $0.97 < \kappa_W < 1.3$ (68% CL) (black band Fig. 2, right-hand side). A heavier resonance mass is also necessary, with $M_V = M_A > 1.8$ TeV (68% CL).

Finally, in the inverted-mass scenario, we obtain the upper bound $\kappa_W < 2$ (68% CL) for $1 < M_V/M_A < 2$. Nonetheless, if no vector resonance is seen below the TeV ($M_V > 1$ TeV) the scalar coupling becomes again constrained to be around $\kappa_W \simeq 1$ for $1 < M_V/M_A < 2$, with the 68% CL interval $0.7 < \kappa_W < 1.9$. The outcomes for various mass splittings in the different scenarios with only the 1st WSR (normal-ordered, degenerate and inverted-mass) can be observed in Fig. 2.

In summary, contrary to what is sometimes stated, the current electroweak precision data easily allow for resonance states at the natural EW scale, *i.e.*, well over the TeV. The present results are in good agreement with the $H \rightarrow WW, ZZ$ couplings measured at LHC, compatible with the Standard Model up to deviations of the order of 20% or smaller [18]). These conclusions are generic, since we have only used mild assumptions about the UV behavior of the underlying strongly-coupled theory, and can be easily particularized to more specific models obeying the $SU(2)_L \otimes SU(2)_R \rightarrow SU(2)_{L+R}$ EWSB pattern.

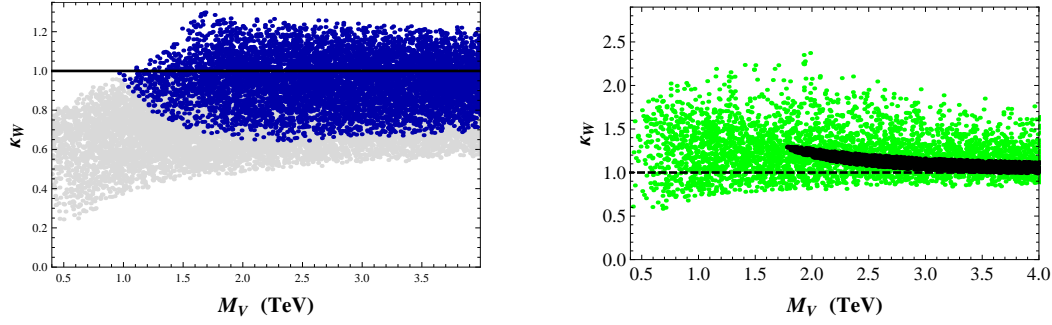


Figure 2: **Left-hand side:** Scatter plot for the 68% CL region, in the case when only the 1st WSR is assumed, for $M_V < M_A$. The dark blue and light gray regions correspond, respectively, to $0.2 < M_V/M_A < 1$ and $0.02 < M_V/M_A < 0.2$. **Right-hand side:** 68% CL region with only the 1st WSR for the degenerate and inverted-hierarchy scenarios. The black (dark) and green (lighter) regions correspond, respectively, to $M_V = M_A$ and $1 < M_V/M_A < 5$. We consider $M_{V,A} > 0.4$ TeV in both plots.

References

- [1] M. E. Peskin and T. Takeuchi, Phys. Rev. D **46** (1992) 381; Phys. Rev. Lett. **65** (1990) 964.
- [2] M. Baak *et al.*, Eur. Phys. J. C **72** (2012) 2205; <http://gfitter.desy.de/>.
- [3] A. Pich, I. Rosell and J. J. Sanz-Cillero, Phys. Rev. Lett. **110** (2013) 181801; [arXiv:1307.1958 [hep-ph]].
- [4] A. Pich, I. Rosell and J.J. Sanz-Cillero, [arXiv:1310.3121 [hep-ph]].
- [5] T. Appelquist and C. W. Bernard, Phys. Rev. D **22** (1980) 200; A. C. Longhitano, Phys. Rev. D **22** (1980) 1166; Nucl. Phys. B **188** (1981) 118.
- [6] A. Dobado, D. Espriu and M. J. Herrero, Phys. Lett. B **255** (1991) 405.
- [7] S. Matsuzaki *et al.*, Phys. Rev. D **75** (2007) 073002; 075012; R. Barbieri *et al.*, Phys. Rev. D **78** (2008) 036012; O. Catà and J.F. Kamenik, Phys. Rev. D **83** (2011) 053010; A. Orgogozo and S. Rychkov, JHEP **1306** (2013) 014.
- [8] A. Orgogozo and S. Rychkov, JHEP **1203** (2012) 046;
- [9] A. Pich, I. Rosell and J.J. Sanz-Cillero, JHEP **0701** (2007) 039; JHEP **1102** (2011) 109.
- [10] A. Pich, I. Rosell and J. J. Sanz-Cillero, JHEP **0807** (2008) 014.
- [11] A. Pich, I. Rosell and J. J. Sanz-Cillero, JHEP **1208** (2012) 106.
- [12] R. Barbieri *et al.*, Nucl. Phys. B **409** (1993) 105.
- [13] C. W. Bernard *et al.*, Phys. Rev. D **12** (1975) 792.
- [14] S. Weinberg, Phys. Rev. Lett. **18** (1967) 507.
- [15] M. Knecht and E. de Rafael, Phys. Lett. B **424** (1998) 335.
- [16] T. Appelquist and F. Sannino, Phys. Rev. D **59** (1999) 067702.
- [17] D. Marzocca, M. Serone and J. Shu, JHEP **1208** (2012) 013 [arXiv:1205.0770 [hep-ph]].
- [18] ATLAS Collaboration, Phys. Lett. B **726** (2013) 88; ATLAS-CONF-2013-079 (July 19, 2013); CMS Collaboration, JHEP **06** (2013) 081; CMS-PAS-HIG-13-005 (April 17, 2013).